Robust and Decoupling Approach to PID Control of Vapour-compression Refrigeration Systems ⋆

David Rodríguez *, **Guillermo Bejarano** *, **José A. Alfaya** *, and **Manuel G. Ortega** *

* *Department of Systems Engineering and Automatic Control, University of Seville, Camino de los Descubrimientos, no number, E-41092 Seville, Spain (e-mails:* {drgarcia, gbejarano, jalonso9, mortega}@us.es*).*

Abstract:
This paper presents a combined approach to the design of PID control applied to vapour-compression refrigeration systems. The underlying controller consists of two decentralised PIDs, aiming to control both the reference on the temperature of the evaporator secondary fluid, imposed by the cooling demand, and the degree of superheating, by manipulating the compressor speed and the expansion valve. A partial decoupling matrix is calculated to reduce the high coupling between the controlled variables, while the PIDs are tuned applying affine parameterisation and considering the condition for robust stability given by the study on the uncertainty sources and the estimation of the uncertainty region around a nominal linear model. The designed controller is applied to the system proposed in the *Benchmark process challenge* and some comparative simulations are presented and discussed, while the performance indices of the proposed controller with respect to the reference one are analysed.

Keywords: Vapour-compression refrigeration, Uncertain linear systems, Decoupling, Robust stability, PID control

1. INTRODUCTION

Nowadays, energy demand related to refrigeration systems has become an essential element in the overall energy mix. Heating, Ventilating, and Air Conditioning (HVAC) systems are widely used in industrial, commercial, and domestic sectors (Rasmussen et al., 2005; Acosta et al., 2011). Indeed, their weight in energy balance may be up to 30% of the total consumed energy around the world (Castilla et al., 2010; Jahangeer et al., 2011).

Cold-energy production via vapour-compression systems is definitively the most common method used worldwide. The basic cycle makes use of a refrigerant to remove heat from the secondary fluid at the evaporator, working at low pressure, then this heat is transferred to the environment or another secondary fluid at the condenser, working at higher pressure and temperature. Compressor and expansion valve are the elements in charge of increasing/decreasing the refrigerant pressure and closing the inverse Rankine cycle, and they represent the two main manipulated variables.

Significant efforts focused on incrementing energy efficiency while reducing environmental impact of current vapour-compression systems have been carried out in the last years. The conventional control scheme is applied as follows: in addition to the reference on the temperature of the evaporator secondary fluid ($T_{e,sec,out}$) imposed by the cooling demand, a low but constant set point on the degree of superheating (T_{SH}) of the refrigerant at the evaporator outlet is applied. Then, the controller is designed to get these two variables to track their references as efficiently as possible in presence of disturbances by manipulating the compressor speed N and the expansion valve opening A_v.

In this context, the *Benchmark process challenge* hosted by the PID 2018 Conference allows to approach this stimulating control problem in order to test new developments in the design of PID controllers. Indeed, decentralised PID control represents a very used linear technique in this field (Wang et al., 2007; Marcinichen et al., 2008; Salazar and Méndez, 2014). Furthermore, given that the main difficulty when controlling this process lies in high thermal inertia, dead times, high coupling between variables, and strong non-linearities, more complex techniques recently proposed are based on decoupling (Shen et al., 2010; Morilla et al., 2013) and robust control (Larsen and Holm, 2003; Bejarano et al., 2015; Alfaya et al., 2015).

In this paper a combination of the three referenced techniques is developed. The underlying controller consists of two decentralised PIDs, as expressed in the scope of the PID 2018 Conference, but partial decoupling is previously applied, since the coupling between the two controlled variables turns out to be relevant, as clarified later. Furthermore, when modelling a refrigeration system linearly, strong non-linearities and disturbances arise and

⋆ This work was supported by MCeI (Grant DPI2015-70973-R).

they could lead to closed-loop instability when applying a linear controller. If the latter was robust enough, it could deal with those issues, despite its linearity, even at operating points further from the design point. Then, a multivariable linear model is proposed and identified at the nominal operating point proposed in the *Benchmark process challenge*, while possible uncertainty at different operating points and that related to frequency and sampling time are discussed, estimating the uncertainty region. Later, the decentralised PIDs are tuned using affine parameterisation, also taking into account the condition for robust stability, calculated considering the estimated uncertainty region around the nominal point. Simulations comparing the reference controller of the *Benchmark process challenge* and the proposed one are presented and discussed. Moreover, in the light of the results issued by the proposed controller, the performance indices generated by the quantitative comparison are analysed.

The rest of the paper is organised as follows: Section 2 describes the linear modelling at the nominal point, whereas Section 3 analyses the uncertainty sources and shows the estimation of the multiplicative output uncertainty. The partial decoupling strategy and the relation with the estimated uncertainty are clarified in Section 4, while Section 5 details the controller design using affine parameterisation. The comparative simulations and performance indices of the proposed controller are analysed in Section 6. Eventually, the main conclusions to be derived are summarised in Section 7.

2. LINEAR MODELLING

Firstly, given the nominal operating point defined in the *Benchmark process challenge*, the step-response method is applied to identify a low-order linear model expressed as a transfer matrix $\boldsymbol{G}(s)$, as shown in (1). A static gain, k_{ij}, a dominating zero, $\tau_{z_{ij}}$, and two poles (one fast, $\tau_{f_{ij}}$, and another one slower, $\tau_{s_{ij}}$) are considered for every transfer function $G_{ij}(s) \quad \forall i,j = 1,2$. Fig. 1 shows the step response of the system at the nominal operating point.

$$\begin{bmatrix} \Delta T_{e,sec,out}(s) \\ \Delta T_{SH}(s) \end{bmatrix} = \boldsymbol{G}(s) \begin{bmatrix} \Delta A_v(s) \\ \Delta N(s) \end{bmatrix}$$
$$\boldsymbol{G}(s) = \begin{bmatrix} \frac{k_{11}(\tau_{z_{11}}s+1)}{(\tau_{f_{11}}s+1)(\tau_{s_{11}}s+1)} & \frac{k_{12}(\tau_{z_{12}}s+1)}{(\tau_{f_{12}}s+1)(\tau_{s_{12}}s+1)} \\ \frac{k_{21}(\tau_{z_{21}}s+1)}{(\tau_{f_{21}}s+1)(\tau_{s_{21}}s+1)} & \frac{k_{22}(\tau_{z_{22}}s+1)}{(\tau_{f_{22}}s+1)(\tau_{s_{22}}s+1)} \end{bmatrix} \quad (1)$$

Note the high coupling between the variables to be controlled, with the exception of the influence of the compressor speed N on the outlet temperature of the evaporator secondary fluid $T_{e,sec,out}$, as shown in the upper right subplot of Fig. 1. The *Relative Gain Array* (RGA) method is used to justify the decoupling and find out the most suitable input-output matching (Bristol, 1966). The evaluation of the relationship between the system static gains and the closed-loop ones is proposed, as shown in (2), where $k_{C_{ij}} \quad \forall i,j = 1,2$ represent the closed-loop static gains and $\boldsymbol{\lambda}$ is the relative gain matrix.

$$\begin{bmatrix} k_{11} & k_{12} \\ k_{21} & k_{22} \end{bmatrix} = \begin{bmatrix} -0.017 & 0.0016 \\ -0.24 & 0.15 \end{bmatrix}$$
$$\begin{bmatrix} \frac{1}{k_{C_{11}}} & \frac{1}{k_{C_{12}}} \\ \frac{1}{k_{C_{21}}} & \frac{1}{k_{C_{22}}} \end{bmatrix} = \left(\begin{bmatrix} k_{11} & k_{12} \\ k_{21} & k_{22} \end{bmatrix}^{-1} \right)^T \quad (2)$$
$$\boldsymbol{\lambda} = \begin{bmatrix} \frac{k_{11}}{k_{C_{11}}} & \frac{k_{12}}{k_{C_{12}}} \\ \frac{k_{21}}{k_{C_{21}}} & \frac{k_{22}}{k_{C_{22}}} \end{bmatrix} = \begin{bmatrix} 1.1773 & -0.1773 \\ -0.1773 & 1.1773 \end{bmatrix}$$

As stated by Bristol, the best input-output matching is that achieving the elements closest to 1 in matrix $\boldsymbol{\lambda}$. Therefore, the *RGA* method confirms that the best input-output pairs are $\{T_{e,sec,out}, A_v\}$ and $\{T_{SH}, N\}$. However, according to the static-gain elements obtained in (2), A_v has a great influence on T_{SH}, thus the partial decoupling strategy is expected to reduce this issue.

3. UNCERTAINTY ANALYSIS AND ESTIMATION

One of the main uncertainty sources of the nominal model is that related to variability of the system dynamics far

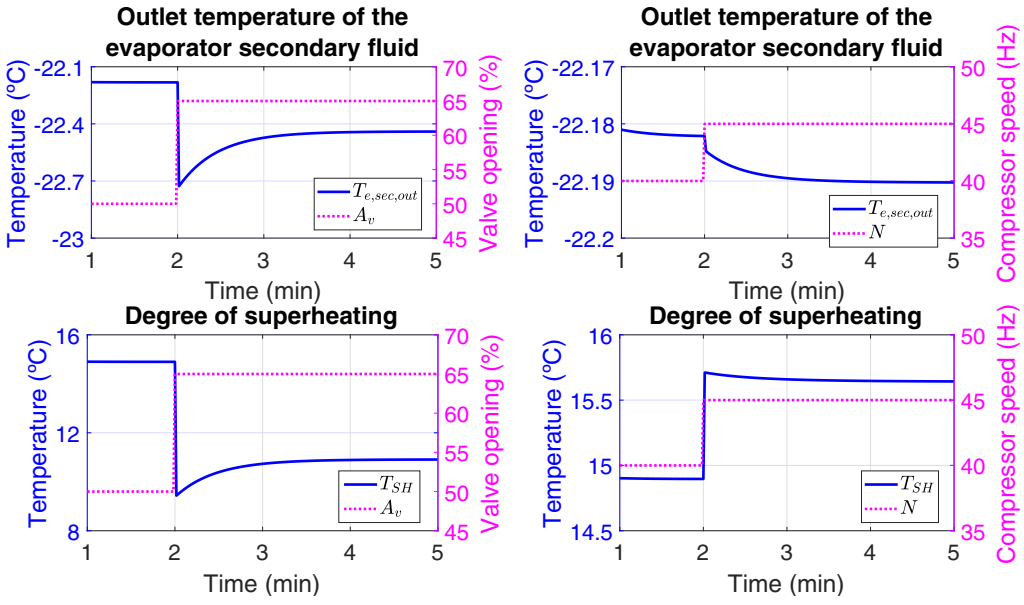

Fig. 1. Step response of the system at the nominal operating point

away from the nominal operating point. That is why a number of non-nominal operating points have been defined according to the expected variations of the manipulated variables around the nominal values. All of them are described in Table 1. Similarly, low-order linear transfer matrices $\boldsymbol{G}_{OPi}(s)$ have been identified at every non-nominal operating point OP_i ($\forall i = 1, 2, ..., 4$), as that shown in (1).

Table 1. Selected operating points

Operating point	N(Hz)	A_v(%)
Nominal	40	50
OP_1	50	60
OP_2	30	60
OP_3	50	40
OP_4	30	40

Other potential uncertainty sources are not parametric, as that considered regarding the non-nominal operating points, but structural. For instance, the linear model is expected to be uncertain at high frequency, as well as around frequencies close to that corresponding to the sampling time. The controller is intended to be designed far from these frequencies, where the system dynamics are not well described by the linear model.

The procedure proposed by some works in the literature (Ortega and Rubio, 2004; Ortega et al., 2007) has been applied to estimate the uncertainty region, according to the previously identified transfer matrices at a series of non-nominal operating points. First, the nominal model must be adjusted in scale, according to the maximum deviation of each input and output. Equation (3) shows how the scaled model $\hat{\boldsymbol{G}}(s)$ is calculated from the input and output scaling matrices, $\boldsymbol{D_u}$ and $\boldsymbol{D_y}$, respectively.

$$\hat{\boldsymbol{G}}(s) = \boldsymbol{D_y^{-1}}\ \boldsymbol{G}(s)\ \boldsymbol{D_u} \tag{3}$$

Then, the maximum singular values σ_{max} of the multiplicative output uncertainty $\hat{\boldsymbol{E}}_{OP_i}(j\omega)$ can be computed as indicated in (4), where $\hat{\boldsymbol{G}}_{OP_i}(j\omega)$ refers to the frequency response of the identified linear model at the operating point OP_i ($\forall i = 1, 2, ..., 4$), once scaled. The calculated maximum singular values are represented along frequency in Fig. 2.

$$\sigma_{max}(\hat{\boldsymbol{E}}_{OP_i}(j\omega)) = \sigma_{max}((\hat{\boldsymbol{G}}_{OP_i}(j\omega) - \hat{\boldsymbol{G}}(j\omega))\ \hat{\boldsymbol{G}}(j\omega)^{-1}) \tag{4}$$

The multiplicative output uncertainty imposes a frequency constraint on the achievable control bandwidth. Therefore, the controller is intended to be designed in such a way that it satisfies the condition for robust stability shown in (5), where $\boldsymbol{T}(s)$ represents the output complementary sensitivity transfer matrix and $\boldsymbol{W_T}(s)$ denotes its weighting transfer matrix. The latter can be computed as a diagonal matrix, as shown in (6), where $W_{T_{diag}}(s)$ is the tightest enveloping transfer function meeting (7) for every non-nominal model and frequency, whose magnitude is also shown in Fig. 2.

$$\begin{aligned} &||\boldsymbol{W_T}(s)\ \boldsymbol{T}(s)||_\infty \leqslant 1 \\ &|\boldsymbol{T}(j\omega)| \leqslant \left|\boldsymbol{W_T^{-1}}(j\omega)\right| \quad \forall\omega \end{aligned} \tag{5}$$

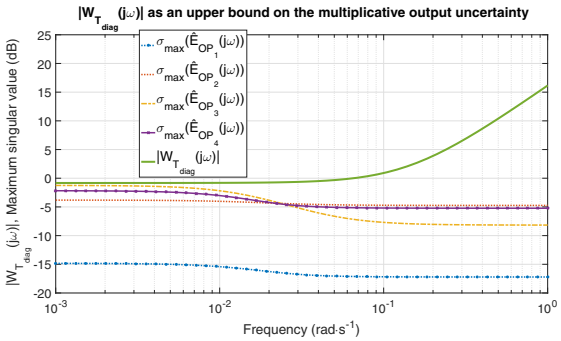

Fig. 2. Maximum singular values of the multiplicative output uncertainty and the weighting transfer function $W_{T_{diag}}(j\omega)$

$$\boldsymbol{W_T}(s) = W_{T_{diag}}(s)\ \boldsymbol{I}_2 \tag{6}$$

$$\left|W_{T_{diag}}(j\omega)\right| \geqslant \sigma_{max}(\hat{\boldsymbol{E}}_{OP_i}(j\omega)) \quad \forall\omega,\ \forall OP_i \tag{7}$$

Note that, as commented before, the linear models identified at the non-nominal operating points by means of the step-response method are expected not to represent correctly the system dynamics from frequencies greater than 10^{-1} rad/s, considering the sampling time. That is the reason why the enveloping transfer function $W_{T_{diag}}(s)$ has been calculated in such a way that its magnitude grows along frequency from these frequencies on, thus ensuring (7) despite the uncertainty in the description of the system dynamics.

4. DECOUPLING AND RELATION WITH UNCERTAINTY

Given the relevant coupling between the two controlled variables shown in Fig 1, a partial decoupling strategy is addressed. Three traditional control options can be found in the literature (Morilla et al., 2013): pure decentralised control, decentralised control combining with a partial decoupling net, and centralised control. On one hand, regarding the pure decentralised strategy, each output is to be controlled by the most suitable input and each controller is designed either ignoring its influence over the remaining outputs or considering the whole information of the multivariable process model. On the other hand, the centralised strategy aims to design a multivariable controller that considers all crossed influence. In this paper the second strategy is addressed, where a decoupling matrix $\boldsymbol{D}(s)$ is placed between the controller $\boldsymbol{C}(s)$ and the system $\boldsymbol{G}(s)$ (see Fig. 3). This matrix $\boldsymbol{D}(s)$ is conveniently calculated in such a way that the design of monovariable controllers for every output can be carried out. Note that, in Fig. 3, $G_{ij}(s)\ \ \forall i, j = 1, 2$ represents each element of the transfer matrix $\boldsymbol{G}(s)$ shown in (1), $D_{ij}(s)\ \ \forall i, j = 1, 2$ denotes each element of the partial decoupling matrix $\boldsymbol{D}(s)$, and $C_{11}(s)$ and $C_{22}(s)$ are the monovariable controllers at the intended diagonal controller matrix $\boldsymbol{C}(s)$. The appropriate input-output matching for partial decoupling has been chosen by the RGA method explained before.

The partial decoupling matrix is obtained by solving (8), where $\boldsymbol{G^*}(s)$ is the desired diagonal transfer matrix which is intended to be used in the design of monovariable

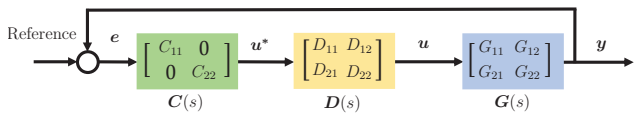

Fig. 3. Decoupling strategy

controllers. The proposed solution is stated in (9), where $D_{11}(s)$ and $D_{22}(s)$ have been selected as one to hold the original diagonal transfer functions $G_{11}(s)$ and $G_{22}(s)$ unaltered. Note that $G_{12}(s)$ is neglected when calculating the partial decoupling matrix $\boldsymbol{D}(s)$, taking into account the small value of the corresponding static gain k_{12}.

$$\boldsymbol{G}(s)\boldsymbol{D}(s) = \begin{bmatrix} G_{11} & G_{12} \\ G_{21} & G_{22} \end{bmatrix} \begin{bmatrix} D_{11} & D_{12} \\ D_{21} & D_{22} \end{bmatrix} = \boldsymbol{G}^*(s) = \begin{bmatrix} G_{11}^* & 0 \\ 0 & G_{22}^* \end{bmatrix} \tag{8}$$

$$\boldsymbol{D}(s) = \begin{bmatrix} D_{11} & D_{12} \\ D_{21} & D_{22} \end{bmatrix} \approx \begin{bmatrix} 1 & 0 \\ -\frac{G_{21}}{G_{22}} & 1 \end{bmatrix} \tag{9}$$

Furthermore, the estimation of the multiplicative output uncertainty performed in Section 3 is not influenced by the partial decoupling matrix, as stated in (10). Considering again the scaled representation and undoing the variable change $\hat{\boldsymbol{G}}^*(s) = \hat{\boldsymbol{G}}(s)\boldsymbol{D}(s)$, it is shown that the partial decoupling matrix turns out to be cancelled, since it is the same for every scaled transfer matrix $\hat{\boldsymbol{G}}(s)$ and $\hat{\boldsymbol{G}}_{OP_i}(s)$.

$$\begin{aligned} \hat{\boldsymbol{E}}_{OP_i}(j\omega) &= (\hat{\boldsymbol{G}}^*_{OP_i}(j\omega) - \hat{\boldsymbol{G}}^*(j\omega))\hat{\boldsymbol{G}}^*(j\omega)^{-1} \; = \\ &= (\hat{\boldsymbol{G}}_{OP_i}(j\omega)\boldsymbol{D}(j\omega) - \hat{\boldsymbol{G}}(j\omega)\boldsymbol{D}(j\omega))(\hat{\boldsymbol{G}}(j\omega)\boldsymbol{D}(j\omega))^{-1} = \\ &= [\hat{\boldsymbol{G}}_{OP_i}(j\omega) - \hat{\boldsymbol{G}}(j\omega)]\boldsymbol{D}(j\omega)\boldsymbol{D}(j\omega)^{-1}\hat{\boldsymbol{G}}(j\omega)^{-1} \; = \\ &= [\hat{\boldsymbol{G}}_{OP_i}(j\omega) - \hat{\boldsymbol{G}}(j\omega)]\hat{\boldsymbol{G}}(j\omega)^{-1} \quad \forall i = 1, 2, ..., 4 \end{aligned} \tag{10}$$

5. CONTROLLER DESIGN

Once estimated the multiplicative output uncertainty and calculated the transfer function $W_{T_{diag}}(s)$, which represents an upper bound on the mentioned uncertainty, the decentralised PIDs are to be tuned using affine parameterisation. The output complementary sensitivity transfer matrix $\boldsymbol{T}(s)$ can be calculated as indicated in (11), where $\boldsymbol{Q}(s)$ is the transfer matrix to be designed in order to achieve the desired closed-loop behaviour. The matrix $\boldsymbol{Q}(s)$ can be expressed as indicated in (12), as long as the diagonalised nominal transfer matrix $\boldsymbol{G}^*(s)$ can be inverted, using an auxiliary transfer matrix $\boldsymbol{F_Q}(s)$. Note that the controller design procedure is like that of the monovariable case, despite the matrix formulation included in (11) and (12), where all matrices are diagonal.

$$\boldsymbol{T}(s) = \boldsymbol{Q}(s)\, \boldsymbol{G}^*(s) \tag{11}$$

$$\boldsymbol{Q}(s) = \boldsymbol{F_Q}(s)\, \boldsymbol{G}^{*-1}(s) \Rightarrow \boldsymbol{T}(s) = \boldsymbol{F_Q}(s) \tag{12}$$

$\boldsymbol{F_Q}(s)$ must be selected in such a way that $\boldsymbol{Q}(s)$ is stable and proper. Moreover, the condition for robust stability shown in (5) is imposed. Therefore, the designed $\boldsymbol{T}(s)$ must hold below its weighting transfer matrix $\boldsymbol{W_T^{-1}}(s)$. $\boldsymbol{T}(s)$ is designed as shown in (13), where identical first-order transfer functions have been selected for both output variables, only characterised by the time constant τ. Three different controller tunings are proposed, according to the value of τ. The output complementary sensitivity transfer function $T_{T_{e,sec,out}}(s)$ and the weighting transfer function $W_{T_{diag}}(s)$ are shown in Fig. 4, for the three controller tunings. Note that $T_{T_{SH}}(s)$ is not represented in Fig. 4, since it matches $T_{T_{e,sec,out}}(s)$, as stated in (13).

$$\boldsymbol{T}(s) = \boldsymbol{F_Q}(s) = \begin{bmatrix} T_{T_{e,sec,out}}(s) & 0 \\ 0 & T_{T_{SH}}(s) \end{bmatrix} = \begin{bmatrix} \frac{1}{\tau s+1} & 0 \\ 0 & \frac{1}{\tau s+1} \end{bmatrix} \tag{13}$$

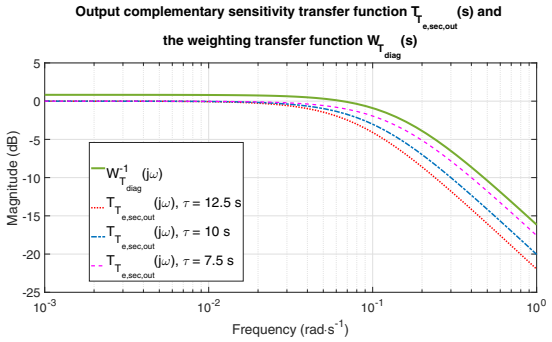

Fig. 4. Output complementary sensitivity transfer function $T_{T_{e,sec,out}}(s)$ and the weighting transfer function $W_{T_{diag}}(s)$, for the three controller tunings

It is shown in Fig. 4 that the output complementary sensitivity transfer functions hold below the weighting transfer function, which makes the designed controllers robust. According to the affine parameterisation, the controller $\boldsymbol{C}(s)$ to be applied is calculated as shown in (14), giving rise to two PID controllers with a first-order filter, as shown in the general formulation indicated in (15). The values of the controller parameters are detailed in Table 2, where it is observed that the controller on $T_{e,sec,out}$ presents the whole formulation shown in (15), whereas that controlling T_{SH} turns out to be a PI controller without the filter. Note also that the value of τ only modifies the proportional gain. An anti-windup scheme has been also included after the application of the partial decoupling matrix.

$$\boldsymbol{C}(s) = (\boldsymbol{I}_2 - \boldsymbol{Q}(s)\, \boldsymbol{G}^*(s))^{-1}\, \boldsymbol{Q}(s) = \begin{bmatrix} C_{11}(s) & 0 \\ 0 & C_{22}(s) \end{bmatrix} \tag{14}$$

$$C_{ii}(s) = k_p \frac{T_i T_d s^2 + T_i s + 1}{T_i s} \frac{1}{\tau_{flt} s + 1} \quad \forall i = 1, 2 \tag{15}$$

6. SIMULATION RESULTS AND CONTROLLER COMPARISON

In this section the performance of the proposed controller is compared, both qualitatively and quantitatively, to the reference one provided in the formulation of the

Table 2. Controller parameters

Controller tunings		$\tau = 12.5$ s	$\tau = 10$ s	$\tau = 7.5$ s
$C_{11}(s)$	k_p ($\% \cdot \mathrm{K}^{-1}$)	-124.70	-155.88	-207.84
	T_i (s)	26.5	26.5	26.5
	T_d (s)	0.49	0.49	0.49
	τ_{flt} (s)	56.5	56.5	56.5
$C_{22}(s)$	k_p ($\mathrm{Hz} \cdot \mathrm{K}^{-1}$)	0.533	0.667	0.889
	T_i (s)	0.95	0.95	0.95
	T_d (s)	0	0	0
	τ_{flt} (s)	0	0	0

Benchmark process challenge. Fig. 5 and 6 show the controlled variables and their set points, considering the reference controller and the three different controllers designed in Section 5, for the given profiles including changes in the references and disturbances $T_{e,sec,in}$ and $T_{c,sec,in}$. Fig. 7 and 8 represent the manipulated variables, while Table 3 gathers the relative performance indices and the combined index evaluated for all designed controllers with respect to the reference one, as described in the main document of the *Benchmark process challenge*.

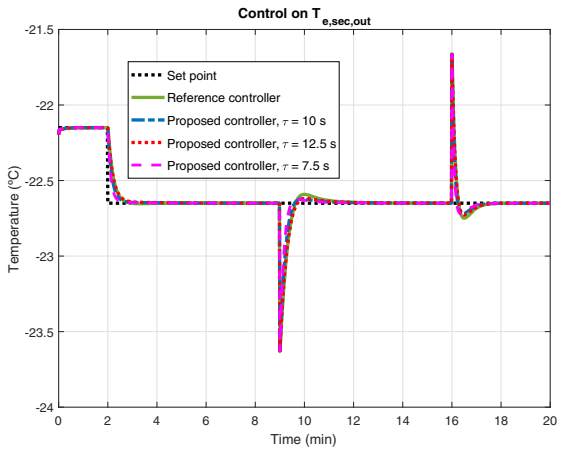

Fig. 5. Controlled variables. Tracking of the set point on the outlet temperature of the evaporator secondary fluid

It can be noticed in Fig. 5-8 and Table 3 that the proposed controllers considering $\tau = 10$ s and $\tau = 7.5$ s outperform the reference controller, improving almost all relative performance indices. The best one is that featuring $\tau = 7.5$ s, which only worsens slightly the $RIAVU_1$ index with respect to the reference controller while improving significantly the remaining ones and thus the combined index. However, all proposed controllers improve both $RIAE$ indices and the overshooting is quite reduced in both controlled variables, as shown in Fig. 5 and 6. Moreover, the proposed controllers avoid the saturation of the compressor speed N when rejecting the last disturbance on the inlet temperature of the condenser secondary fluid $T_{c,sec,in}$ at $t = 16$ min, as depicted in Fig. 8.

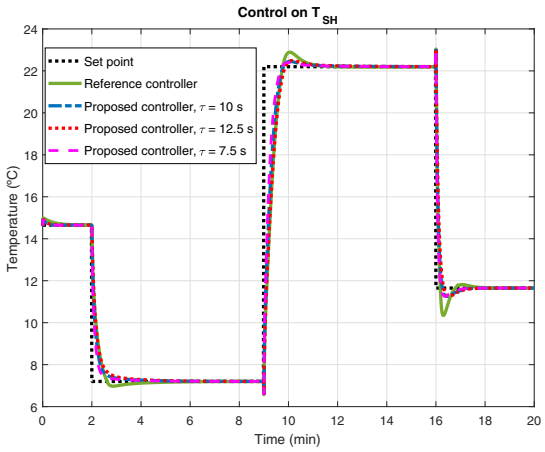

Fig. 6. Controlled variables. Tracking of the set point on the degree of superheating

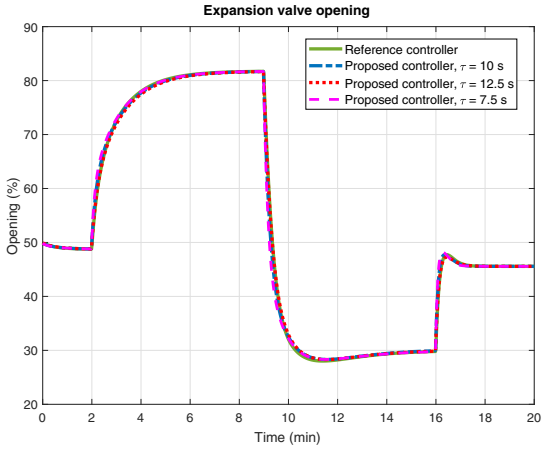

Fig. 7. Manipulated variables. Expansion valve opening

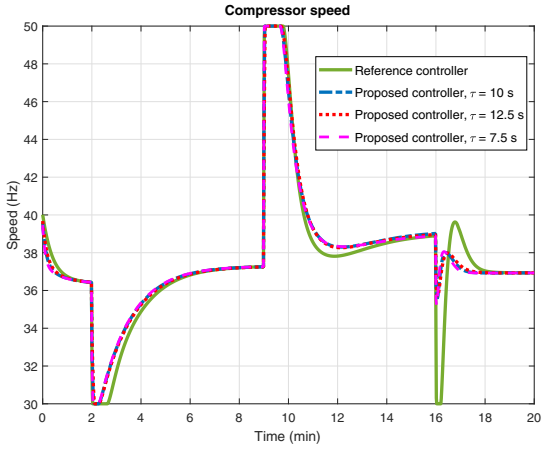

Fig. 8. Manipulated variables. Compressor speed

7. CONCLUSIONS

In this paper a combined approach to the design of multivariable PID controllers has been proposed, considering the *Benchmark process challenge* hosted by the PID 2018 Conference about the control of vapour-compression re-

Table 3. Relative performance indices of the proposed controllers

Relative indices	$\tau = 12.5$ s	$\tau = 10$ s	$\tau = 7.5$ s
$RIAE_1(C_2, C_1)$	0.9286	0.7724	0.6046
$RIAE_2(C_2, C_1)$	0.9722	0.8193	0.6563
$RITAE_1(C_2, C_1, t_{c1}, t_{s1})$	1.9260	1.3780	0.8932
$RITAE_2(C_2, C_1, t_{c2}, t_{s2})$	1.1226	0.8208	0.5561
$RITAE_2(C_2, C_1, t_{c3}, t_{s3})$	0.9189	0.7115	0.5043
$RITAE_2(C_2, C_1, t_{c4}, t_{s4})$	0.7303	0.5891	0.4297
$RIAVU_1(C_2, C_1)$	0.9850	0.9931	1.0012
$RIAVU_2(C_2, C_1)$	0.7554	0.7591	0.7661
$J(C_2, C_1)$	**1.1517**	**0.8994**	**0.6600**

frigeration systems. Firstly, a partial decoupling matrix has been calculated to limit the influence of every monovariable controller over the remaining variable, whereas the application of the *Relative Gain Array* method has provided the best input-output matching between controlled and manipulated variables. Secondly, an uncertainty analysis has been performed on an identified nominal model, whose main uncertainty sources have been evaluated. The uncertainty region has been estimated and the monovariable controllers have been tuned using affine parameterisation, taking into account the condition for robust stability imposed by the uncertainty analysis. The design procedure leads to a classical PID formulation with a first-order filter. Three different controller tunings have been proposed and their performance has been compared to that of the reference controller provided in the formulation of the *Benchmark process challenge*, achieving better performance indices and improving the overall dynamic behaviour of the controlled variables. Further work would include the application of the developed strategy to the experimental cycle, as well as including feedforward action to the controller output, considering the measurable disturbances such as the secondary temperatures.

REFERENCES

Acosta, A.V., González, A.I., Zamarreño, J.M., and Álvarez, V. (2011). A hotel building model for energy prediction. *RIAI - Revista Iberoamericana de Automática e Informática Industrial*, 8(4), 309–322. doi: 10.1016/j.riai.2011.09.001.

Alfaya, J.A., Bejarano, G., Ortega, M.G., and Rubio, F.R. (2015). Controllability analysis and robust control of a one-stage refrigeration system. *Eur. J. of Control*, 26, 53–62. doi:10.1016/j.ejcon.2015.08.001.

Bejarano, G., Alfaya, J.A., Ortega, M.G., and Rubio, F.R. (2015). Multivariable analysis and H_∞ control of a one-stage refrigeration cycle. *Appl. Therm. Eng.*, 91, 1156–1167. doi:10.1016/j.applthermaleng.2015.09.003.

Bristol, E.H. (1966). On a new measure of interaction for multivariable process control. *IEEE Trans. on Autom. Control*, 11, 133–134. doi:10.1109/TAC.1966.1098266.

Castilla, M., Álvarez, J., Berenguel, M., Pérez, M., Rodríguez, F., and Guzmán, J. (2010). Técnicas de control del confort en edificios. *RIAI - Revista Iberoamericana de Automática e Informática Industrial*, 7(3), 5 – 24. doi:10.4995/RIAI.2010.03.01.

Jahangeer, K.A., Tay, A.A.O., and Islam, M.R. (2011). Numerical investigation of transfer coefficients of an evaporatively-cooled condenser. *Appl. Therm. Eng.*, 31(10), 1655–1663. doi: 10.1016/j.applthermaleng.2011.02.007.

Larsen, L.S. and Holm, J.R. (2003). Modelling and multivariable control of refrigeration systems. *ECOS 2003*.

Marcinichen, J., del Holanda, T., and Melo, C. (2008). A dual SISO controller for a vapor compression refrigeration system. In *12th Int. Refrig. and Air Cond. Conf., at Purdue, West Lafayette-IN, USA*.

Morilla, F., Garrido, J., and Vázquez, F. (2013). Multivariable control by decoupling. *RIAI - Revista Iberoamericana de Automática e Informática Industrial*, 10, 3–17. doi:10.1016/j.riai.2012.11.001.

Ortega, M.G., Castaño, F., Vargas, M., and Rubio, F.R. (2007). Multivariable robust control of a rotary dryer: Analysis and design. *Control Eng. Pract.*, 15(4), 487–500. doi:10.1016/j.conengprac.2006.09.005.

Ortega, M.G. and Rubio, F.R. (2004). Systematic design of weighting matrices for H_∞ mixed sensitivity problem. *J. of Process Control*, 14(1), 89–98. doi:10.1016/S0959-1524(03)00035-0.

Rasmussen, B.P., Musser, A., and Alleyne, A.G. (2005). Model-driven system identification of transcritical vapor compression systems. *IEEE Trans. on Control Syst. Technol.*, 13, 444–451. doi:10.1109/TCST.2004.839572.

Salazar, M. and Méndez, F. (2014). PID control for a single-stage transcritical CO_2 refrigeration cycle. *Appl. Therm. Eng.*, 67(1), 429–438. doi: 10.1016/j.applthermaleng.2014.03.052.

Shen, Y., Cai, W.J., and Li, S. (2010). Normalized decoupling control for high-dimensional MIMO processes for application in room temperature control HVAC systems. *Control Eng. Pract.*, 18(6), 652–664. doi: 10.1016/j.conengprac.2010.03.006.

Wang, J., Zhang, C., Jing, Y., and An, D. (2007). Study of neural network PID control in variable-frequency air-conditioning system. In *IEEE Int. Conf. on Control and Autom.*, 317–322. doi:10.1109/ICCA.2007.4376371.